



¹Simmons University, Boston, MA

²Louisiana Cancer Research Center, New Orleans, LA

³Department of Cell and Molecular Biology, School of Science and Engineering, Tulane University, New Orleans, LA

⁴Department of Physiology, School of Medicine, Tulane University, New Orleans, LA

Introduction

- Angiogenesis is the process of new blood vessel formation from existing vessels. It is critical for embryonic development and wound repair, and it is essential for solid tumor progression and metastasis.
- We propose that endothelial cells are activated during angiogenesis to undergo partial endothelial-to-mesenchymal transition (pEndoMT) under control of master transcription factors Slug, Snail, Twist, Ovof1, and Ovof2.^{1,2}

Hypothesis

Lentiviral constructs can drive constitutive overexpression of transcription factors that drive Endothelial-to-Mesenchymal Transition (pEndoMT) – e.g., Slug, Snail, Ovof1, and Ovof2 – in endothelial cells.

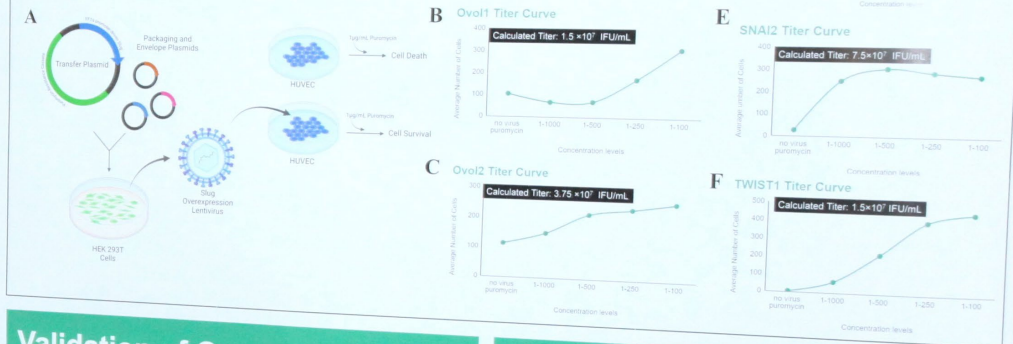
Overexpression of pEndoMT transcription factors will affect extent of sprouting angiogenesis.

Methods

- We generated Generation III lentivirus from published plasmids³ to overexpress pEndoMT transcription genes in Human Umbilical Vein Endothelial Cells (HUVECs).
- Lentivirus was made in Human Embryonic Kidney (HEK) 293T packaging cells.
- Lentivirus was quantitatively titered in HUVEC by measuring dose-dependent puromycin resistance.
- Constitutive overexpression of pEndoMT transcription factors was confirmed in transduced HUVEC using quantitative PCR (qPCR).

Determination of Lentiviral Titer via Puromycin Resistance

Figure 1. Calculating Lentiviral Titer. A) Schematic of lentiviral production in 293T packaging cells, and transduction into HUVEC for quantification of viral titer by dose-dependent puromycin resistance. Figure generated in Biorender.com. Transduced HUVEC survival curves at 4 days following addition of puromycin were generated for overexpression lentiviruses for B) Ovof1, C) Ovof2, D) SNAI1 (Snail), E) SNAI2 (Slug), and F) TWIST1 (TWIST). Using these curves, we were able to calculate the concentration of infectious units (IFU) for each lentivirus.



Validation of Overexpression

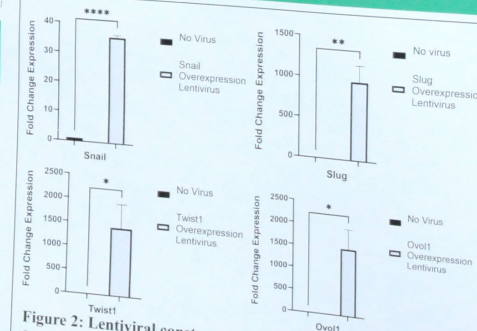
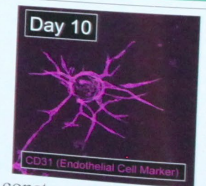


Figure 2: Lentiviral constructs drive constitutive transcription factor overexpression in HUVEC. HUVEC were transduced with lentiviral constructs (MOI = 1), and RNA was isolated after 4 days of transduction. Quantitative PCR (qPCR) was used to measure SNAI1 (Snail), SNAI2 (Slug), TWIST1 (Twist), and OVOL1 (Ovof1). Basal OVOL2 (Ovof2) expression was undetectable, thus a fold change could not be calculated for this gene.

Future Directions

Figure 3: Representative image of sprouting angiogenesis in Fibrin Gel Bead Assay. HUVEC cultured on collagen-coated beads sprout under angiogenesis in 3D fibrin hydrogel.



- Perform additional validation of our lentiviral overexpression constructs.
- Use Fibrin Gel Bead Assay to test if pEndoMT transcription factor overexpression in HUVEC alters sprouting angiogenesis.
- Use Tumor Angiogenesis-on-a-Chip platform to test if pEndoMT transcription factor overexpression in HUVEC alters tumor angiogenesis.

References

- Fang, J. S., Hullgren, N. W., & Hughes, C. C. (2021). Regulation of partial and reversible endothelial-to-mesenchymal transition in angiogenesis. *Frontiers in Cell and Developmental Biology*, 9, doi:10.3389/fcell.2021.702021
- Roca, H., Hernandez, J., Weidner, S., McEachin, R. C., Fuller, D., Sud, S., ... Pienta, K. J. (2013). Transcription factors OVOL1 and OVOL2 induce the mesenchymal to epithelial transition in human cancer. *PLoS ONE*, 8(10), doi:10.1371/journal.pone.0076773
- Juang, J., Ma, S., Geiger-Scheller, K.R., Kirchgatterer, P.C., Verdine, V.K., ... Zhang, F. (2023). A transcription factor atlas of directed differentiation. *Cell*, 186(1), 209-229. doi: 10.1016/j.cell.2022.11.026.

This research project was supported by the Stanley S. Scott Cancer Center, and by an LCRC New Investigator Award (Fang).

Role of DNA Methyltransferases and EZH2 in Enzalutamide Resistant Prostate Cancer

Brandon E. Burrow^{1,5}, Santosh Lamichhane^{1,4,5}, Sweaty Koul^{1,3,5} and Hari K Koul^{1,2,3,4,5}

Departments of ¹Interdisciplinary Oncology, ²Biochemistry & Molecular Biology, ³Urology, LSUHSC-New Orleans; ⁴Southeast Louisiana Veterans Health Care System, New Orleans - LA; and ⁵LSU-LCMC Cancer Center, School of Medicine, Louisiana State University Health Sciences Center, New Orleans, LA, USA

Introduction

Prostate cancer is the most prevalent malignancy among men in the United States, resulting in over 35,000 deaths annually (1). It originates primarily from the luminal epithelial cells of the prostate gland, which arise from basal cells during prostate development and differentiation and are characterized by the expression of the androgen receptor (AR) and other specific markers. While androgen signaling is essential for the normal function and survival of luminal cells, it is also pivotal in the development and progression of prostate cancer (6).

Androgen deprivation therapy (ADT) has long been a cornerstone in the treatment of advanced prostate cancer. By reducing levels of androgens, ADT aims to inhibit androgen receptor signaling and therefore reduce the growth and proliferation of prostate cancer cells (5). However, despite the initial efficacy of ADT, most patients eventually develop resistance, leading to the emergence of castration-resistant prostate cancer (CRPC). Enzalutamide (ENZ), a next-generation AR inhibitor, has been approved by the FDA for treating metastatic CRPC (mCRPC). It works by inhibiting the androgen receptor signaling pathway. Clinical trials have demonstrated that ENZ extends overall survival and delays disease progression (2).

However, the majority of patients who initially respond to ENZ eventually develop resistance, known as Enzalutamide Resistance (ENZ-R).

ENZ-R is marked by adaptive cellular mechanisms, including the emergence of neuroendocrine prostate cancer (NEPC) and the emergence of neuroendocrine prostate cancer (NEPC-ONPC) phenotypes. These have been extensively investigated in ENZ-R, the role of which is less understood. Recent studies, including those by Lamichhane et al. (3), have identified increased expression and activity of DNA methyltransferases (DNMT1, DNMT3a, and DNMT3b) and the histone H3K27 methyltransferase (EZH2) during prostate cancer resistance to ENZ. The role of DNMTs in ENZ-R has not been fully elucidated.

The potential of DNMT and EZH2 inhibitors to overcome ENZ-R is being explored. DNMT inhibitors, such as 5-Aza-2'-deoxycytidine (5-AZA-dC), which incorporates into DNA and covalently traps DNMT, leading to its degradation and reactivation of silenced genes, GSK-260981 (GSK-260981) which inhibits the methyltransferase activity of histone H3 on lysine 27 (H3K27me3), which is a key marker of ENZ-R. Our results show that targeting these epigenetic enzymes may overcome ENZ-R in Prostate Cancer.

Methods

ENZ-R cell lines were cultured under standard conditions receiving consistent treatment with 5μM ENZ. Protein levels of DNMT and other prostate cancer markers were quantified through Western blotting techniques.

Cell growth and proliferation were monitored using the IncuCyte live-cell analysis system. Cells were seeded into 96-well plates and monitored for 96 hours. Cell density was quantified through the IncuCyte live-cell analysis system.

Cells were seeded into 96-well plates and monitored for 96 hours. Cell density was quantified through the IncuCyte live-cell analysis system.

Cells were seeded into 96-well plates and monitored for 96 hours. Cell density was quantified through the IncuCyte live-cell analysis system.

Cells were seeded into 96-well plates and monitored for 96 hours. Cell density was quantified through the IncuCyte live-cell analysis system.

Cells were seeded into 96-well plates and monitored for 96 hours. Cell density was quantified through the IncuCyte live-cell analysis system.

Cells were seeded into 96-well plates and monitored for 96 hours. Cell density was quantified through the IncuCyte live-cell analysis system.

Cells were seeded into 96-well plates and monitored for 96 hours. Cell density was quantified through the IncuCyte live-cell analysis system.

Cells were seeded into 96-well plates and monitored for 96 hours. Cell density was quantified through the IncuCyte live-cell analysis system.

Fig 2. Enzalutamide Resistance is associated with increased DNMT Expression

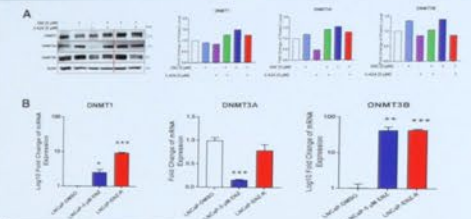


Fig 2. Enzalutamide Resistance is associated with increased DNMT Expression. Panel A: Protein levels of DNMT1, DNMT3A, and DNMT3B were assessed in LNCaP and LNCaP-ENZ-R cell lines treated with 5 μM ENZ, 5 μM 5-AZA, or a combination of both. Actin was used as a loading control. Fig 2a. Quantification of Protein Expression: Bar graphs representing the quantification of DNMT1, DNMT3A, and DNMT3B protein levels from the Western blot data. The graphs show relative protein expression normalized to actin in LNCaP and LNCaP-ENZ-R cells under different treatment conditions; 2b: Gene Expression Analysis: PCR quantification of DNMT1, DNMT3A, and DNMT3B mRNA levels in LNCaP and LNCaP-ENZ-R cell lines under the same treatment conditions as in (A). The results are presented as log10 fold changes relative to untreated controls. Statistical significance is indicated (*p < 0.05, **p < 0.01, ***p < 0.001).

Fig 3. Enz-Resistant PCa cells are sensitive to DNMT inhibition, and Inhibition of DNMT sensitizes PCa cells to ENZ

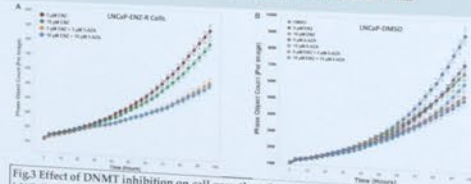


Fig 3. Effect of DNMT inhibition on cell growth and proliferation: 3a: Cell Growth in LNCaP-ENZ-R Cells treated with varying concentrations of ENZ (5 μM and 10 μM), 5-AZA (5 μM and 10 μM), and their combinations were monitored 96 hours using the IncuCyte live-cell analysis system; 3b: The growth and proliferation of LNCaP-ENZ-R cells treated with varying concentrations of ENZ (5 μM and 10 μM), 5-AZA (5 μM and 10 μM), and their combinations were monitored 96 hours using the IncuCyte live-cell analysis system. Cell Density: 3k

Fig 4. Inhibition of DNMT's decreased clonogenic activity of ENZ-Resistant PCa cells



Fig 4. Effects of DNMT inhibition on Colony Formation: A: Representative images of colonies formed by LNCaP cells following treatment with 5 μM ENZ, 5 μM 5-AZA, and 5 μM ENZ + 5 μM 5-AZA. B: Representative images of colonies formed by LNCaP-ENZ-R cells following treatment with 5 μM ENZ, 5 μM 5-AZA, and 5 μM ENZ + 5 μM 5-AZA. The bar graph below indicates a significant reduction in colony formation in LNCaP-ENZ-R cells treated with combination of ENZ and 5-AZA. Statistical significance is indicated (*p < 0.05, ***p < 0.001).

These studies suggest DNMT and EZH2 activities as a potential therapeutic vulnerability that can be exploited for limiting cellular plasticity, tumor progression, and therapy resistance in prostate cancer. Because DNMT and EZH2 inhibitors are currently approved for other malignancies, addition of these inhibitors to current treatment regimens could be readily explored in PCa.

Fig 5. Enzalutamide Resistance is associated with increased EZH2 Expression

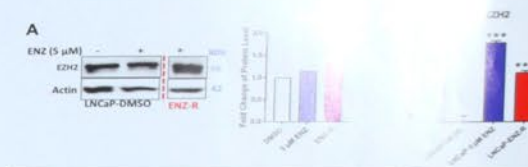


Fig 5. Effect of Enzalutamide on EZH2 Levels: A) Protein expression levels of EZH2 were assessed in LNCaP and LNCaP-ENZ-R cell lines treated with 5 μM ENZ. Actin was used as a loading control, and the quantification of EZH2 protein levels from the Western blot data; B: EZH2 mRNA levels in LNCaP and LNCaP-ENZ-R cell lines were measured via Realtime PCR. The results are presented as log10 fold changes relative to untreated controls. (**p < 0.01, ***p < 0.001).

Fig 6. PCa cells are sensitive to the inhibition of DNMT and EZH2: Dual inhibition of DNMT's and EZH2 decreased growth and proliferation of ENZ-R-PCa cells

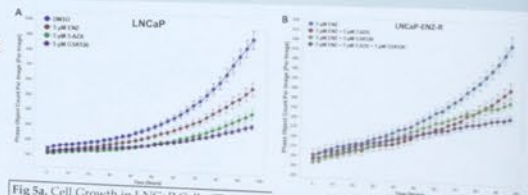


Fig 6a. Cell Growth in LNCaP Cells: The proliferation of LNCaP cells treated with 5 μM ENZ, 5 μM 5-AZA, 5 μM GSK126, and their combinations were monitored over 96 hours using the IncuCyte live-cell analysis system. Fig 6b. Cell Growth in LNCaP-ENZ-R Cells: The proliferation of LNCaP-ENZ-R cells under the same treatment conditions as in (A) was monitored similarly.

Conclusions:

Our data demonstrated that the DNA and Histone methylation pathways are deregulated in ENZ-R Prostate cancer cell lines, and that targeting DNA methyltransferases and EZH2 sensitized the prostate cancer cells enzalutamide (current treatment).



These studies suggest DNMT and EZH2 activities as a potential therapeutic vulnerability that can be exploited for limiting cellular plasticity, tumor progression, and therapy resistance in prostate cancer. Because DNMT and EZH2 inhibitors are currently approved for other malignancies, addition of these inhibitors to current treatment regimens could be readily explored in PCa.

References

1. American Cancer Society (2018). Prostate cancer. Retrieved from: <https://www.cancer.org/cancer/prostate-cancer/about/prostate-cancer-key-statistics.html>
2. Chen Y, Tang Y, Lam S, Meng X, Guo X, Jiang L, et al. (2017). The differential androgen activity of 5-Aza-2'-deoxycytidine in prostate cancer cell lines. *Journal of Cancer* 8(12): 2279-2286.
3. Lamichhane S, Koul S, Koul H, Koul H, Koul H, Koul H, et al. (2018). The differential androgen activity of 5-Aza-2'-deoxycytidine in prostate cancer cell lines. *Journal of Cancer* 9(12): 2279-2286.
4. Koul S, Koul H, Koul H, Koul H, Koul H, Koul H, et al. (2018). The differential androgen activity of 5-Aza-2'-deoxycytidine in prostate cancer cell lines. *Journal of Cancer* 9(12): 2279-2286.
5. Koul S, Koul H, Koul H, Koul H, Koul H, Koul H, et al. (2018). The differential androgen activity of 5-Aza-2'-deoxycytidine in prostate cancer cell lines. *Journal of Cancer* 9(12): 2279-2286.
6. Koul S, Koul H, Koul H, Koul H, Koul H, Koul H, et al. (2018). The differential androgen activity of 5-Aza-2'-deoxycytidine in prostate cancer cell lines. *Journal of Cancer* 9(12): 2279-2286.

Introduction

Synovial fibrosis (Sfb), a painful contracture limiting joint motion and quality of life, is a hallmark of arthrofibrosis (AF), a common complication after joint repair. Sfb is categorized by low (<41%), moderate (42-54%), and high (>54%) collagen deposition levels and is a significant challenge in osteoarthritis (OA) patients. As shown in Figure 1, transforming growth factor beta 1 (TGFβ1) drives Sfb and regulates essential cell processes. Interleukin (IL) 11, synthesized downstream of the TGFβ1-mediated JAK/STAT3 cascade, promotes fibrosis if dysregulated. Novomedix's (NMX) novel inhibitors selectively target IL11 without disrupting TGFβ1-mediated functions. These inhibitors effectively reduce IL11-driven collagen deposition in OA-derived fibrotic synoviocytes.

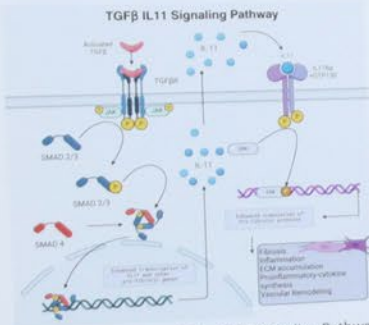


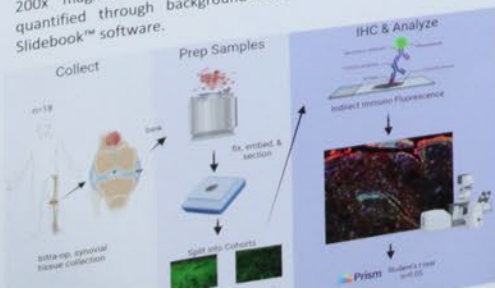
Figure 1: The TGFβ1 mediated IL11 Signaling Pathway

Objective and Significance

To assess the potential of NMX for in vivo Sfb treatment, this study analyzes IL11 co-expression with TGFβ1 in banked knee OA samples, hypothesizing a correlation between IL11 expression and Sfb severity.

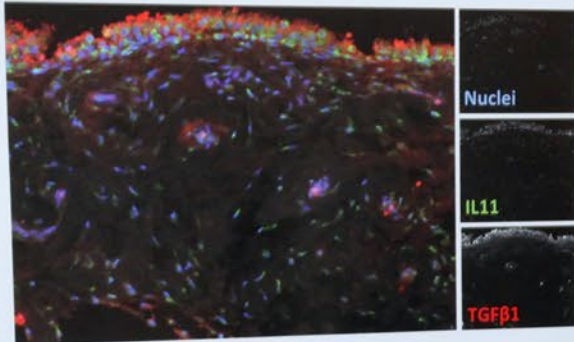
Methods

Sfb cohorts were based on pre-defined histological scores. Co-detection of TGFβ1 and IL11 by indirect immunofluorescence used anti-TGFβ1 (mouse monoclonal) and anti-IL11 (rabbit polyclonal) antibodies. Sections were then stained with anti-mouse Alexa 594 and anti-rabbit Alexa 647 secondary antibodies for TGFβ1 and IL11, respectively, along with DAPI nuclear counterstain. Samples were mounted and imaged using a confocal microscope (Olympus) at 200x magnification. Co-expression of TGFβ1 and IL11 was quantified through background-corrected signal analysis using Slidebook™ software.



Results

Low Fibrosis



High Fibrosis

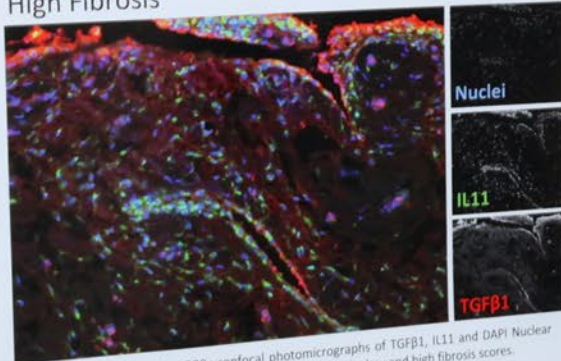


Figure 2: Representative 200x confocal photomicrographs of TGFβ1, IL11 and DAPI Nuclear counterstain in the synovium of KOA patients grouped by low and high fibrosis scores.

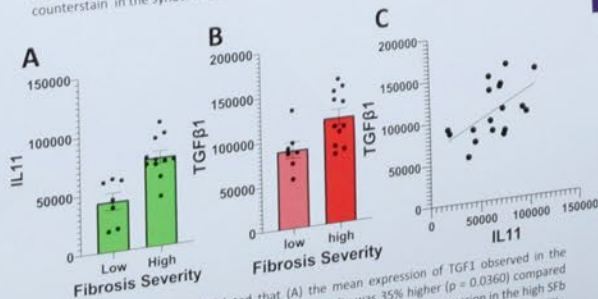


Figure 3: Student T test calculated with high Sfb severity was 35% higher ($p = 0.0360$) compared to the signal measured from the low severity Sfb group and (B) IL11 expression in the high Sfb severity were registered at a 77% increase ($p = 0.0016$) from patients with less severe Sfb. Pearson's correlation revealed (C) a moderate but significant correlation between TGFβ1 and IL11 ($R = 0.51$; $p = 0.0314$).

Discussion and Limitations

- Increased expression of IL11 relates to TGFβ1 in agreement with Sfb severity. While this study does not prove causality, it suggests a relationship between IL11 and Sfb, highlighting the diseased synovium as an effective target for NMX administration.
- The study is limited by sample size and doesn't account for confounding variables such as synovitis grade and presence of additional pro-fibrotic factors such as connective tissue growth factor.
- Further studies will investigate the effectiveness of NMX on aberrant collagen deposition, contraction, and myofibroblast differentiation rate of patient-derived synovial fibroblasts.

Conclusion

- IL11 levels in patient synovial tissue correlate to TGFβ1 levels and severity of Sfb. While this study does not prove causality, it provides further evidence that IL11 and Sfb are interrelated.
- Further studies will investigate the effectiveness of the NMX compound in patient synovial tissue.
- This study indicates the potential supplementation of NMX to assist manipulation under anesthesia and arthroscopic lysis of adhesions in the management of debilitating arthrofibrosis.

Acknowledgements

We would like to thank members of the Morphology and Imaging Laboratory and the Morphology and Imaging Laboratory for their technical assistance and thoughtful discussions. We also thank the LSU Integrated Musculoskeletal Biobank (LIMB) for the use of the LIMB used in study was supported by an award from the LSU Health Research Enhancement Program. We thank Dr. Marrero for your constant guidance and support that has made this project possible.

References

- Blaney Davidson EN, van der Kraak PM, van den Broek P, et al. Osteoarthritis and osteoarthritis. Osteoarthritis and cartilage. 2007;15(6):597-604. doi:10.1016/j.joca.2007.02.001
- Schäfer S, Viswanathan S, Widge AA, et al. IL-11 is a determinant of cardiovascular fibrosis. Nature. 2017;552(7683):110-115. doi:10.1038/nature24678
- Ng ET. Interleukin-11 signaling underlies parenchymal dysfunction and chronic inflammation in airway. Experimental & Molecular Medicine. 2020;52(1):1-15.
- Geng ET. PD-L1 on invasive fibroblasts drives fibrosis in a humanized model of idiopathic pulmonary fibrosis. JCI. 2019;129(1):1-15.
- Hodgeson S, O'Brien S, Simkin J, Piskotarski E, McCarthy C, V. Marrero L. Differences in synovial fibrosis relative to range of motion in knee osteoarthritis patients. J Orthop Res. 2019;37(10):2584-2594. doi:10.1002/jor.25061. Epub 2017 May 10. PMID: 28913554. PMCID: PMC5353814.

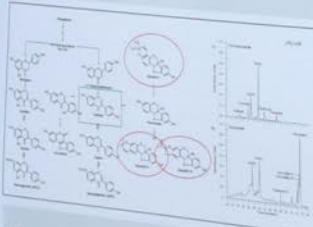
Abstract

For women worldwide, breast cancer (BC) ranks top 2 in both annual quantity of cases and deaths among cancers. Leading these statistics, developing new methods for combating breast cancer remains at the forefront of cancer research. Types of breast cancer are differentiated based on the presence of 3 receptors: estrogen receptor (ER), progesterone receptor (PR), and human epidermal growth factor receptor 2 (HER2). HER2+ BC targeted agents such as trastuzumab, pertuzumab, and lapatinib, alone or in combination with traditional chemotherapeutics, have become the standard of care for this BC subtype, significantly improving patient survival rates. However, the development of resistance to targeted therapy represents a major obstacle in the treatment of HER2+ breast cancer, highlighting a critical need to identify novel therapeutic targets to treat resistant HER2+ breast cancer.

Isoflavonoids, an important class of natural compounds produced from numerous plant sources including legumes, have been identified to be beneficial for human health. A member of the legume family, the soybean, maintains a high isoflavonoid content, specifically daidzein and stress induced derivatives called glyceollins. Recent studies have demonstrated glyceollin activity against ER+ breast cancer due to inhibition of ER and its associated pathways. To date the impact of glyceollins on other breast cancer subtypes has not been fully explored. Here, we utilized a panel of HER2+ breast cancer cell lines (HCC 1954, AU565, SKBR3), as well as derived trastuzumab-resistant variants (herein-resistant SKBR3), to evaluate the effects of glyceollin treatment, alone or in combination with other targeted agents, on cell viability and clonogenicity. Additionally, we analyzed changes in downstream gene expression using qRT-PCR and array for Human Cancer Pathways to define potential glyceollin-targeted pathways involved in the regulation of HER2 breast cancer cell biology.

Results demonstrated that glyceollin decreased cell survival and colony formation across cell lines. Additionally, glyceollin suppressed expression of pro-oncogenic genes in herein-resistant SKBR3 cells. Our preliminary findings provide support for a novel approach using isoflavonoids in the development of targeted therapy for HER2+ BC.

Glyceollin Biosynthesis



Methods Overview



Reduction of Cell Viability

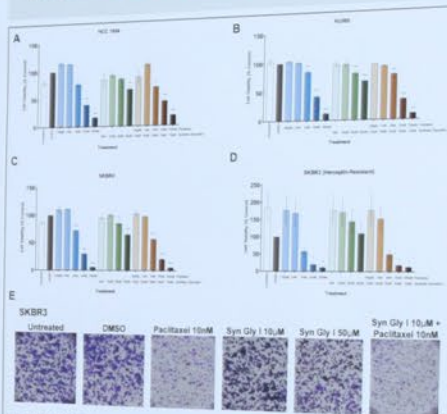


Figure 2. Effects of paclitaxel and synthetic glyceollin I alone or combination treatment on viability of HER2+ cell lines. HER2+ cell lines (A) HCC 1954, (B) AU565 mCherry, SKBR3 (C) parental and (D) herein-resistant SKBR3 were plated on 96-well costar flat-bottom plates (96 cells per well for all cell lines) except AU565 at 10K cells per well. Cells were treated with vehicle (DMSO), paclitaxel, and synthetic glyceollin I (Syn Gly I) alone or in combination. On day 3 post treatment, plates were fixed and stained with crystal violet (E (SKBR3)). Plates were imaged for cell morphology analysis using the BioTek Cytation 5 (Imaging Reader (CY)). Plates were eluted with acetic acid then read at 590nm on the CY. Data shown represent mean \pm SEM, $n=3$. * p -value < 0.05 , ** $p < 0.01$, *** $p < 0.001$.

Effects on colony formation

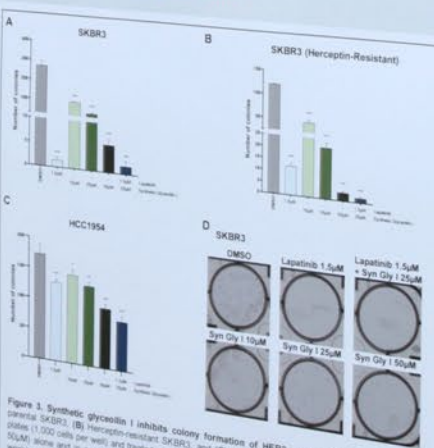


Figure 3. Synthetic glyceollin I inhibits colony formation of HER2+ cells. HER2+ cell lines (A) parental SKBR3, (B) herein-resistant SKBR3, and (C) HCC 1954 were plated on 6-well flat bottom plates (1,000 cells per well) and treated with vehicle, lapatinib, or synthetic glyceollin I (10 μ M, 25 μ M, and 50 μ M) alone and in combination. Cells were cultured until colonies of 50-500 cells formed (at least one well) and imaged using the CY. Graphs were generated with GraphPad Prism software. Data shown represent average number of colonies \pm SEM, $n=3$. * p -value < 0.05 , ** $p < 0.01$, *** $p < 0.001$.

Differential Gene Expression



Figure 4. Cancer pathway analysis of cells treated with synthetic glyceollin I. HER2+ cell lines HCC 1954, AU565, mCherry, parental SKBR3, and herein-resistant SKBR3 were treated with synthetic glyceollin I (25 μ M) for 24 hours. RNA was extracted from cell pellets using the Zymo Research Quick-RNA MiniPrep Kit. RNA samples were evaluated using a Nanodrop, and cDNA was synthesized via the Qiagen RT First Strand Kit cDNA Synthesis Kit. Gene expression was assessed using the Qiagen Human Cancer Pathway Finder PCR Array Plate. PCR array plates were run on the CFX Opus 96 RT-PCR System, and heat maps were generated using GraphPad Prism software.

Conclusions and Future Directions

Conclusions

- Synthetic glyceollin I treatment significantly inhibits proliferation and viability of HER2+ breast cancer cells in a dose-dependent manner.
- Expression of cancer-related genes was altered in HCC1954 cells treated with Syn Gly I, notably TEK which is involved in angiogenesis.
- The majority of genes in the cancer pathway PCR array were downregulated in Syn Gly I-treated herein-resistant SKBR3 cells compared to herein-responsive cells, suggesting enhanced sensitivity of the former to Syn Gly I treatment.

Future Directions

- Assess effects of Syn Gly I treatment on cell viability and gene expression of additional herein-responsive and -resistant HER2+ cell lines.
- Perform qRT-PCR to validate PCR array gene targets.

Acknowledgements

This work was supported in part by funding from the U.S. Department of Agriculture under Non-Assistance Cooperative Agreement (NACA) agreement no. 58-6054-1-015-USDA Agricultural Research Service (USDA-ARS), with additional support provided by the National Cancer Institute of the National Institutes of Health (3R01CA273095-01S1); the Tulane Cancer Center, part of Tulane Medical School, and a consortium partner of the Louisiana Cancer Research Center.

References

- Bull, R., Das, S., Gunasekaran, V. P., Yadav, A. S., Kumar, D., & Kundu, G. C. (2018). Receptor tyrosine kinases (RTKs) in breast cancer: signaling, therapeutic implications and challenges. *Molecular cancer*, 17(1), 34.
- Huo, J.L., Hung, M.C. The role of HER2, EGFR, and other receptor tyrosine kinases in breast cancer. *Cancer Metastasis Rev* 35, 575–588 (2014).
- Narita, R., Esteva, F.J. HER2 therapy: Molecular mechanisms of trastuzumab resistance. *Breast Cancer Res* 8, 215 (2006).
- Zhong, Y., Shao, H., Jin, J., Wang, Q., Jiang, H., Wang, J., Wu, C., Chen, L., Zou, X., Wang, X., Xue, H., Nannan, J., Glyceollins from soybean: Their pharmacological effects and biosynthetic pathways. *Heliyon* 9, 11 (2023).

This research project was supported by the Stanley S. Scott Cancer

Exploring the impact of alcohol and SIV on skeletal muscle mitochondria in western diet-fed Rhesus Macaques

Elizabeth Ellis, Keishia M. Rodriguez-Graciani Ph.D., Patricia Molina Ph.D., and Luis Simon Ph.D.

LSU Health School of Medicine

Background

Results

Methods

Conclusions

References

Figure 1: Image of Triple Negative Breast

Figure 2: Image of Triple Negative Breast

Figure 3: Image of Triple Negative Breast

Figure 4: Image of Triple Negative Breast

Figure 5: Image of Triple Negative Breast

Figure 6: Image of Triple Negative Breast

Figure 7: Image of Triple Negative Breast

Figure 8: Image of Triple Negative Breast

Figure 9: Image of Triple Negative Breast

Figure 10: Image of Triple Negative Breast

Figure 11: Image of Triple Negative Breast

Figure 12: Image of Triple Negative Breast

Figure 13: Image of Triple Negative Breast

Figure 14: Image of Triple Negative Breast

Figure 15: Image of Triple Negative Breast

Figure 16: Image of Triple Negative Breast

Figure 17: Image of Triple Negative Breast

Figure 18: Image of Triple Negative Breast

Figure 19: Image of Triple Negative Breast

Figure 20: Image of Triple Negative Breast

Figure 21: Image of Triple Negative Breast

Figure 22: Image of Triple Negative Breast

Figure 23: Image of Triple Negative Breast

Figure 24: Image of Triple Negative Breast

Figure 25: Image of Triple Negative Breast

Figure 26: Image of Triple Negative Breast

Figure 27: Image of Triple Negative Breast

Figure 28: Image of Triple Negative Breast

Figure 29: Image of Triple Negative Breast

Figure 30: Image of Triple Negative Breast

Figure 31: Image of Triple Negative Breast

Figure 32: Image of Triple Negative Breast

Figure 33: Image of Triple Negative Breast

Figure 34: Image of Triple Negative Breast

Figure 35: Image of Triple Negative Breast

Figure 36: Image of Triple Negative Breast

Figure 37: Image of Triple Negative Breast

15

Health
NEW ORLEANS

School of Medicine

Development of a Smart Dual Acting Drug Delivery System (SDADDS)

Kayla Gant¹, Mya Jordan¹, Aimee Martin², Susana Ferrufino¹, Stassi DiMaggio¹, Jaya Sridhar¹

¹Department of Chemistry, Xavier University of Louisiana

²Department of Biology, Loyola University of New Orleans

LOUISIANA CANCER
RESEARCH CENTER

Abstract

The present-day challenge of delivering anti-cancer agents selectively to tumor cells to mitigate systemic toxicity has led to greater focus on drug delivery research using nanoscale carriers. Despite progress in preclinical studies, the therapeutic effects have not lived up to their expectations in the clinical setting. Though promising, these systems typically exploit passive delivery of a single therapeutic to the target tissue, for example, by (i) encapsulation of drugs in carrier systems followed by drug release in an external trigger. Our project addresses this issue through the design and synthesis of a Smart Dual Acting Drug Delivery System (SDADDS) consisting of monodisperse bifunctional nanocarriers capable of synergistic targeting of multiple drivers of cancer thereby overcoming current limitations to treating cancer. Triple negative breast cancer (TNBC), accounts for 10-15% of all breast cancers. TNBC is a malignant disease that grows sporadically due to it having no selective actionable dominant target. This has caused no target therapy to be approved, thus making it an excellent model to explore the efficiency of SDADDS.

Figure 1: Image of Triple Negative Breast

Objectives

This study aims to utilize two different modes of cellular targeting synergistically that would not only offer superior therapeutic selectivity for tumor tissues, but would also decrease chemotherapeutic toxicity due to reduced drug dosage. The SDADDS in theory should both target the overexpressed TAM receptors on tumor cells and deliver the therapeutic through nanomaterials to increase the bioavailability and decrease chemotherapeutic toxicity.

Design Mechanism

The SDADDS will comprise of A) extracellular receptor targeting through polyvalent binding to increase selective binding to cancerous cells and B) photolabile linkers that will allow a high local concentration of the anti-neoplastic agent to be released in close proximity to the target tissue through controlled photorelease (Figure 2). RU301/302 (Figure 3) have been identified as inhibitors of AXI receptors which belong to the TAM family. They will first be modified for dendron attachment appropriately to ensure receptor binding and inhibition functions are maintained (Figures 4 and 5). The second step is to ensure that the photolabile dioxanin complex (dendron B) can be controlled through photorelease. Once uncaged, the drug molecule dioxanin will be released locally targeting the Src intracellular pathway. The final step of the strategy is linking the TAM inhibitor and the dioxanin-dendron together to create the bifunctional targeted drug delivery system (SDADDS), that should effectively inhibit growth of the target cancer cells overexpressing TAM receptors.

Figure 3: Load TAM inhibitors RU301 and RU302, repress cellular proliferation

Figure 4: Schematic of the TAM inhibitor, dioxanin, and dendron complex

Figure 5: Schematic of the TAM inhibitor, dioxanin, and dendron complex

Figure 6: Schematic of the TAM inhibitor, dioxanin, and dendron complex

Figure 7: Schematic of the TAM inhibitor, dioxanin, and dendron complex

Figure 8: Schematic of the TAM inhibitor, dioxanin, and dendron complex

Figure 9: Schematic of the TAM inhibitor, dioxanin, and dendron complex

Figure 10: Schematic of the TAM inhibitor, dioxanin, and dendron complex

Synthesis of Fluorescent Dendrimer Model

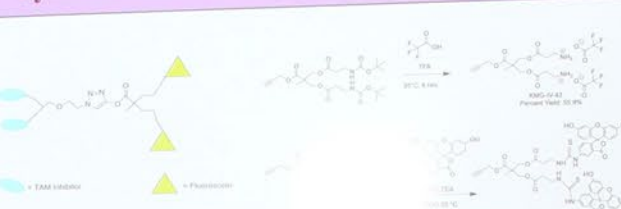


Figure 6: General structure of fluorescent dendrimer functionalized with TAM inhibitor for cellular binding and time lapse studies

Dendron B Analog



Figure 7: ¹H NMR results confirming the deprotection of the dendron (Scheme 1, step 1)



Exploring the Mechanisms of Anticancer Agents with Improved Solubility Against Triple Negative Breast Cancer

LSU Health
NEW ORLEANS
School of Medicine

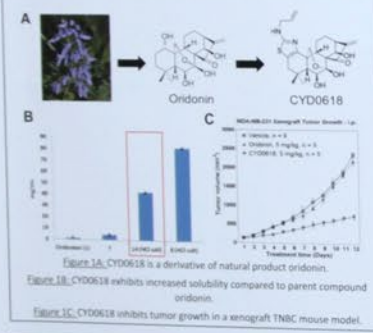
LOUISIANA CANCER RESEARCH CENTER

Paige Goderis, Gabrielle Vontz, Zhipin Liang,
Connor Kent, Lei Liu, Caiyue Li and Qiang Shen
Department of Interdisciplinary Oncology, Louisiana State University Health Sciences Center,
LSU-LCMC Health Cancer Center, New Orleans, LA.

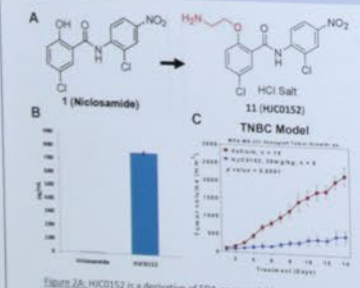
Introduction

Triple-negative breast cancer (TNBC) poses significant challenges in treatment due to its aggressive nature, lack of targeted therapy options, and high resistance rates. TNBC's metabolic dependency on aberrant glycolytic pathways, termed the Warburg effect, provides a potential avenue to develop novel targeted therapies. The Shen Lab investigates mitochondrial and metabolic targets for TNBC to develop innovative anticancer small molecules from synthetic compounds and natural products. Our lab has previously developed a highly soluble derivative of natural product oridonin, CYD0618, that has increased potency against breast cancer in both cell culture experiments and xenograft mouse models. In parallel studies, the lab developed HJC0152, a derivative of FDA-approved antihelminthic niclosamide, that exhibits improved solubility and bioavailability. Despite improvements in potency and bioavailability, specific mechanisms of action of CYD0618 and HJC0152 against breast cancer are understudied. In this project, we evaluated the effects of CYD0618 and HJC0152 on TNBC viability and metabolism using MTT assays, ADP/ATP ratio measurements and Seahorse analysis. Results from this project will contribute to understanding the mechanisms of promising anticancer agents and provide a foundation to optimize these compounds for future clinical testing.

CYD0618



HJC0152



MTT Assays

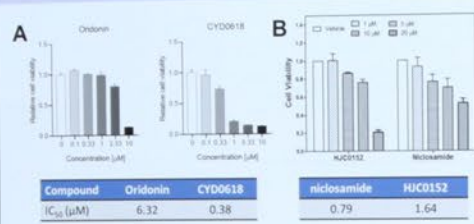


Figure 3A. CYD0618 shows improved potency against TNBC cells in vitro compared to oridonin.
Figure 3B. HJC0152 exhibits comparable potency against TNBC to niclosamide.

ADP/ATP Ratio

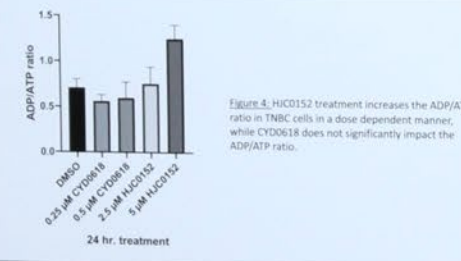


Figure 4. HJC0152 treatment increases the ADP/ATP ratio in TNBC cells in a dose dependent manner, while CYD0618 does not significantly impact the ADP/ATP ratio.

Seahorse Analysis

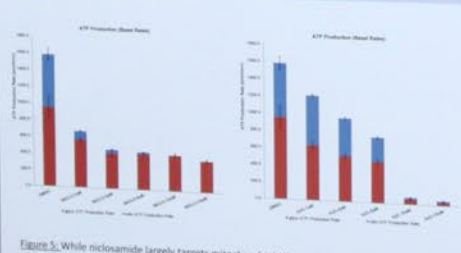


Figure 5. While niclosamide largely targets mitochondrial ATP production, HJC0152 and CYD0618 show different effects on ATP production.

Conclusions

- CYD0618 is derivative of oridonin that exhibits improved solubility and potency against TNBC.
- HJC0152 is a derivative of niclosamide that exhibits improved solubility and bioavailability.
- Both CYD0618 and HJC0152 inhibit TNBC growth in cell culture and xenograft mouse models.
- HJC0152 inhibits ATP production through both mitochondrial phosphorylation and glycolysis.
- CYD0618 and HJC0152 are promising anticancer agents for further investigation for clinical applications.

Future Direction



Figure 6. Degradation based protein profiling (DBPP) to identify direct protein targets of small molecules.

Figure 7. Biotin-labeled tool compounds for further investigation.

Acknowledgments

- This project was supported by the Undergraduate Research Assistant Program at Louisiana Cancer Research Center.
- This project was supported by the R01CA231150 from the National Cancer Institute.
- The derivative of niclosamide was synthesized by the Medical Branch of the University of Texas at Galveston.

How Environmental Risk Factors Drive Racial Disparities in Prostate Cancer Stage Diagnosis

Randy Hamilton¹, Nubaira Rizvi, M.S.², Xiaowen Yang², Michael Celestin Jr., PhD², Ty-Runet Bryant, MPH², Almetra Granger, MPH², Tung Sung Tseng, DrPH², Xiao-Cheng Wu, MD², Qingzhao Yu, PhD²

Xavier University of Louisiana¹, LSU Health Sciences New Orleans²



20

Introduction

- Prostate cancer is the leading cause of cancer among men in the U.S., primarily aged 65 and older.
- In research, prostate cancer shows significant, disproportional effects of 73% higher incidence rates and more than double higher rates of mortality in African American men when compared to Caucasian men.
- Additionally, AA men are diagnosed in younger ages with more aggressive tumors and advanced stages.
- Studies have linked these disparities to be associated with risk factors of socioeconomic, environmental, or biological influencers.
- In our study, we hypothesized environmental factors to be a contributor to the racial disparities in prostate cancer stage at diagnosis between African American and Caucasian men.

Objective

- Identify environmental variables associated with racial disparities in prostate cancer diagnosis outcomes among African American and Caucasian men and quantify their risk.

Methodology

- Data Source:** Louisiana Tumor Registry (LTR) data from 2010 to 2018, 2010 Census Tract data, and Environmental Justice Index (EJI) data.
- Participants:** N=24,647 men in Louisiana; African American (n=8,772 [36%]) and Caucasian (n=15,875 [64%])
- Variables:** Outcome – stage at diagnosis, exposure – African American vs Caucasian, Exploratory Variables - (Marital Status, Insurance, Poverty, CDI, Ozone, Comorbidity, Acetaldehyde, Coal, Cancer Risk, etc.)
- Methods:** Chi-Square test of association, T-Test, ANOVA, and Multiple Mediation Analysis were used to determine our variables' connection to racial disparity in stage
- Analysis:** R Studio



Results

Race	Chi-Square	P-Value	
	10.406	0.001	
*Test of association between stage and race			
	Black/African American (N=8772)	White/ Caucasian (N=15875)	P-value
Stage			0.00126
Early stage	6925 (79.7%)	12771 (80.4%)	
Late stage	1967 (21.3%)	3104 (19.6%)	
Marital Status			<0.001
Married	4593 (52.4%)	10622 (68.2%)	
Not Married	3348 (38.2%)	3291 (20.7%)	
Insurance			<0.001
Private Insurance	2969 (34.1%)	6609 (41.6%)	
Public Insurance	5416 (61.7%)	8472 (53.4%)	
BMI			0.00523
Mean (SD)	29.2 (8.25)	29.4 (5.44)	
Comorbidity			<0.001
0	6765 (77.1%)	13457 (84.8%)	
1 or 2	1736 (19.8%)	2204 (13.9%)	
3 or above	271 (3.1%)	214 (1.3%)	<0.001
Poverty Indicator			<0.001
Mean (SD)	3.49 (0.749)	2.81 (0.917)	
Acetaldehyde			<0.001
Mean (SD)	2920 (14900)	2050 (12500)	
Cancer Risk due to Air Toxics			<0.001
Mean (SD)	0.894 (0.120)	0.858 (0.136)	
% of housing built before 1980 (Lead Exposure)			<0.001
Mean (SD)	59.9 (21.6)	46.7 (22.9)	
Neighborhood Walkability			<0.001
Mean (SD)	7.74 (3.27)	6.75 (2.81)	
Proximity to Railroad (1 mile radius)			<0.001
Mean (SD)	56.6 (37.1)	33.6 (33.4)	
Concentration of Asthma in the Community			<0.001
Mean (SD)	10.7 (1.47)	9.26 (1.13)	
environmental variables between			

Table 1. Comparison of socioeconomic and environmental variables between Black and White patients with p-value.

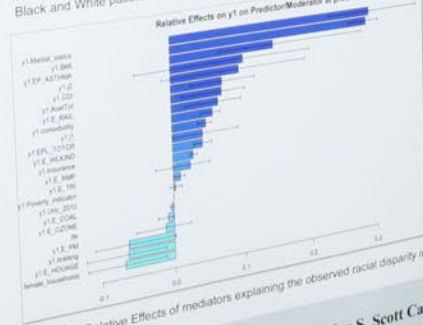


Figure 2: Relative Effects of mediators explaining the observed racial disparity in Prostate cancer patients.

Results (Cont.)

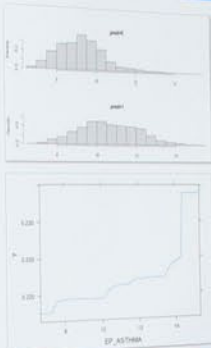


Figure 3: Predi0 is White and Predi1 is Black. Higher proportion of White patients lived in areas where proportion of population with Asthma is low compared to Black patients.

Figure 4: Living in areas with increased proportion of Asthma increases the probability of getting diagnosed at a later stage.

Discussion

- Our investigation found environmental variables to have a partial contribution in explaining the observed racial disparities in prostate cancer stage diagnosis through potential associations in Acetaldehyde (7.1%) and Cancer Risk due to Air Toxics (7.3%).
- Findings in this study were however consistent with previous literature, showing that SES factors such as BMI (35.9%), marital status (31.9%), and insurance (7.3%) provide more significant impact in the disparity of prostate cancer diagnosis when compared to environmental exposure.
- Limitations: No genetic data were collected for the analysis, variables were limited to cancer registry standard data, and a study of African American and Caucasian cancer patients were only able to be considered due the sample size that was too small for other races.

Conclusion

- Environmental risk factors including Acetaldehyde, Concentration of Asthma in the Community, and Cancer Risk due to Air Toxics were identified in contributing an association among racial disparities in prostate cancer stage diagnosis between African American and Caucasian men.
- Further studies should investigate what chemical substances lead to air toxicity and cancer development in neighborhoods to help indicate other associate factors of disparities within cancer diagnosis.

Acknowledgments

The Tobacco Control Initiative and Louisiana Tumor Registry

This research project was supported by the Stanley S. Scott Cancer Center.



"Establishing a 3-D multicellular Tumor Model: Evaluating the impact of fatty acids activated immunosuppressor cells on Breast Cancer spheroid growth"

Madison Jackson, Ramesh Thylur Puttalingaiah Ph.D., Maria Sanchez- Pino, Ph.D.
Louisiana State University Health Sciences, Department of Interdisciplinary Oncology, Stanley S. Scott Cancer Center

Introduction

Background
Obese, 49.3% of the American population were obese. Obesity has been associated with the development of at least 13 types of cancers, including breast cancer in post-menopausal women. The mechanisms behind this association and cancer are unknown. In severe obesity (BMI >40) Oleic Acid (OA) and Palmitic Acid (PA) predominate the circulation and by Linoleic Acid (LA) (~21%).



3D multicellular (EO711 cell line and MDSC) culture was successfully implemented for assessing spheroid growth for 10 days

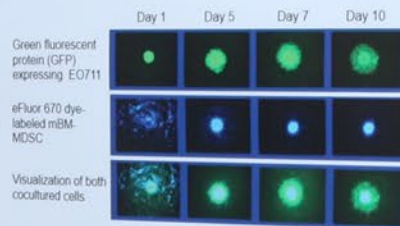


Figure 1: Representative pictures of EO711 spheroids and MDSC during coculture of 10 days. EO711-GFP (10,000 cells) were seeded in a 96-well ultra-low attachment plate. After the formation of a single spheroid, 40,000 eFluor 670 dye-labeled mMDSC were added. The spheroid size was monitored in the Incucyte SX5 for 10 days. Half of the culture media was changed with fresh media at day 6.

MDSC treated with palmitic acid increases the size of EO711 spheroid



Figure 2: Measurements of the green (EO711-GFP) spheroid area after coculture of EO711 spheroid with MDSC induced from mouse bone marrow with recombinant cytokines in the absence (Bovine Serum Albumin [BSA]) or presence of the FFAs BSA-OA, BSA-LA, and BSA-PA.

Differential regulation between different FFA of Arg1 expression without affecting MMP9 and S100A8 protein levels in MDSC

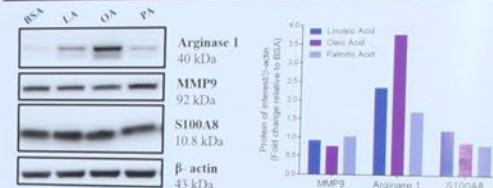


Figure 3: Expression levels of MDSC markers by western blot and densitometry. Cell extract of MDSC treated or not with different FFAs as used to determine the intracellular expression levels of Arg1, MMP9, and S100A8.

Palmitic Acid moderately reduces immunosuppressive function

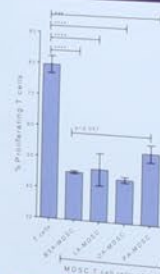


Figure 4: Suppression Assay to evaluate the effect of FFAs on the immunosuppressive function of MDSC on T cell proliferation. Induced MDSC with and without FFAs were cocultured with Cell-Trace violet dye-labeled T-cells for 3 days. Activation of T cells was performed using Dynabeads Mouse T-Activator CD3/CD28 kit in the presence of mouse recombinant IL-2. CellTrace™ dilution on T cell proliferation was measured by flow cytometry.

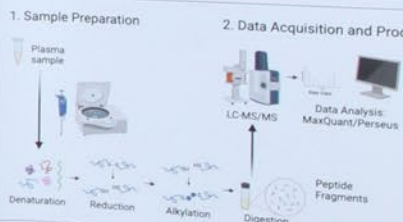
Conclusion & Future Research

- The 3D multicellular culture was successfully established; however, further optimization is needed including 1) the number of seeded cells (EO711 and MDSC), 2) avoiding perturbing spheroids by changing media and 3) not using wells in the borders of the plate due to media evaporation.
- MDSC treated with PA showed a higher capacity for increasing spheroid growth. This PA reduced the expression of Arg1, a marker of immunosuppression, aligns with a decreased capacity to suppress T cell proliferation.
- OA, LA, and PA differentially impact the expression of the MDSC marker Arg1 but not on MMP9 and S100A8.
- Additional assessments need to be performed to determine the effect of FFA on these proteins in supernatant since MMP9 and S100A8 are secreted after activation, as well as other secreted proteins such as cytokines.

Introduction

- Pancreatic cancer is the 3rd-leading cause of cancer death accounting for 66,440 new cases and 51,750 deaths each year, a rate that has increased slowly every year since 2000.
- Roughly 90% of pancreatic cancer cases are pancreatic ductal adenocarcinomas (PDACs) and a vast majority present with a 5-year survival rate of only 11%.
- Early detection of PDAC is currently a crucial, yet challenging task.
- Pancreatitis (acute and chronic) and PDAC have similar risk factors.
- Pancreatitis (inflammation characterized by sustained tissue cellular proliferation, and tissue repair) has been associated with suggested to be an early manifestation or significant risk factor for PDAC.
- Comparisons between protein expression in PDAC and pancreatitis to valuable insight into how the two are connected and the important biomarkers that could be utilized or targeted in the treatment of pancreatic cancer.

Methods



- 30 human plasma samples from 3 different groups were randomly prepared, and analyzed under standard protocol for extraction from plasma for peptide-based liquid chromatography-mass spectrometry (LC-MS).

Sample Group	(1) CTRL (Control group) No diagnosis of PDAC, not presenting with pancreatitis	(2) PAN (Pancreatitis group) No diagnosis of PDAC, presenting with pancreatitis	(3) PDAC (PDAC group) Diagnosis of PDAC
# of Samples (n)	10 (-)	5 (4,1)	1 (6)
Age	Mean: N/A Median: N/A Range: N/A	Mean: 44 Median: 42 Range: 24-63	Mean: 62 Median: 7 Range: 25

Label-Free Quantification (LFQ) intensity data collected from MaxQuant was processed and gap-filled using MaxQuant.

Complete expression ≥ 70% of samples replicates are Expressed	Identified proteins Uncertain expression Between 30% and 70% of replicates are Expressed	No expression ≤ 30% of replicates are Expressed
---------------------------------------------------------------------	------------------------------------------------------------------------------------------------------	----------------------------------------------------------

LSU Health
NEW ORLEANS

“Establishing a 3-D multicellular Tumor Model: Evaluating the impact of fatty acid activated immunosuppressor cells on Breast Cancer spheroid growth”

Madison Jackson, Ramesh Teylur Pottalingiah Ph.D., Maria Sanchez-Pino, Ph.D.
Louisiana State University Health Sciences, Department of Interdisciplinary Oncology, Stanley S. Scott Cancer Center

LOUISIANA CANCER RESEARCH CENTER
SUCRE
SUMMER UNDERGRADUATE CANCER RESEARCH EXPERIENCE

Introduction

Approximately 28.2% of the American population were diagnosed with breast cancer in 2014. Breast cancer has been associated with the consumption of at least 11 types of cancers, including those that are pre-metastatic, metastatic, and those that are post-metastatic. The mechanisms behind the association between obesity and cancer are unclear. Obesity is associated with several chronic diseases, including type 2 diabetes, hypertension, and heart disease. Obesity is also associated with several chronic diseases, including type 2 diabetes, hypertension, and heart disease. Obesity is also associated with several chronic diseases, including type 2 diabetes, hypertension, and heart disease.

3D multicellular (E0711 cell line and MDSC) culture was successfully implemented for assessing spheroid growth for 10 days

Day 1 Day 5 Day 7 Day 10

Figure 1: Representative pictures of E0711 spheroids and MDSC during incubation of 10 days. E0711 (3,000 cells) were seeded in 96-well ultra-low attachment plates. After the formation of a single spheroid, 40,000 of the E0711 (3,000 cells) MDSC were added. The size was measured in the Thermo 555 for 10 days. Half of the media was changed with fresh media at day 5.

Differential regulation between different FFA on Arg1 expression without affecting MMP9 and MMP13 expression in MDSC

Figure 2: Bar graph showing the relative expression of Arg1, MMP9, and MMP13 in MDSC treated with different FFAs. The y-axis represents the relative expression (fold change) and the x-axis represents the treatment groups (Control, LA, OA, and SFA). Arg1 expression is significantly upregulated in the LA and OA groups compared to the control, while MMP9 and MMP13 expression remain relatively unchanged.

LSU Health
NEW ORLEANS

Proteomics Analysis of PDAC and Pancreatitis Plasma Samples: Investigating Associations and Differences

Amelia Jiang-Yu¹, Amirsalar Mansouri^{2,3}, Marek Benes⁴, Mary Maluccio^{2,3}, Nicholas J. Skill^{2,3}, Jiri Adamec^{2,3}

¹Johns Hopkins University, Baltimore, MD, United States
²Louisiana Cancer Research Center, New Orleans, LA, United States
³Louisiana State University – Health Sciences Center, New Orleans, LA, United States
⁴Charles University, 3rd Faculty of Medicine, Prague, Czech Republic

LOUISIANA CANCER RESEARCH CENTER

Introduction

Pancreatic cancer is the 9th leading cause of cancer death in the U.S., accounting for 10,440 new cases and 51,750 deaths each year – a mortality rate that has increased steadily every year since 2008.

Roughly 90% of pancreatic cancer cases are pancreatic ductal adenocarcinoma (PDAC) and a vast majority present at advanced-stage with a 5-year survival rate of only 10%.

Early detection of PDAC is currently a crucial, yet challenging, goal. Pancreatitis (acute and chronic) and PDAC have similar risk factors. Pancreatitis (inflammation characterized by sustained tissue damage, cellular proliferation, and tissue repair) has been associated with and is suggested to be an early manifestation or significant risk factor of PDAC.

Comparisons between protein expression in PDAC and pancreatitis may lead to valuable insight into how the two are connected and the discovery of important biomarkers that could be utilized or targeted in the diagnosis and treatment of pancreatic cancer.

Methods

1. Sample Preparation
2. Data Acquisition and Processing

Figure 1: Schematic diagram of the proteomics workflow. Plasma samples are collected from patients and controls, then processed for protein extraction and digestion. The resulting peptides are analyzed using LC-MS/MS. The data is then processed and analyzed using MaxQuant and Proteome Discoverer.

Figure 2: Venn diagram showing the overlap of protein identifications between PDAC and Pancreatitis. The x-axis represents the number of proteins identified in each group, and the y-axis represents the number of proteins identified in both groups.

Protein Group	Protein Count	Protein Name
Control group	10	Protein A, Protein B, Protein C, Protein D, Protein E, Protein F, Protein G, Protein H, Protein I, Protein J
PDAC group	15	Protein A, Protein B, Protein C, Protein D, Protein E, Protein F, Protein G, Protein H, Protein I, Protein J, Protein K, Protein L, Protein M, Protein N, Protein O
Pancreatitis group	12	Protein A, Protein B, Protein C, Protein D, Protein E, Protein F, Protein G, Protein H, Protein I, Protein J, Protein K, Protein L, Protein M, Protein N, Protein O

Results – Student's T-Test, Hierarchical Clustering

Pairwise comparisons were performed between:

- (A) PDAC vs Controls
- (B) Pancreatitis vs PDAC
- (C) Pancreatitis vs Controls

Figure 1: Heatmap showing the hierarchical clustering of protein expression data. The x-axis represents the protein groups, and the y-axis represents the protein names. The color scale indicates the relative expression level, with red representing high expression and blue representing low expression.

Results – Enriched Pathways

Top 5 Pathways

PDAC vs CTRL	PDAC vs PANC	PANC vs CTRL
1. LXR/RXR Activation	1. Acute Phase Response Signaling	1. Formation of Fibrin Clot (Clotting Cascade)
2. BDNF/RET4 Signaling Pathway	2. Complement cascade	2. Response to elevated platelet cytosolic Ca ²⁺
3. Formation of Fibrin Clot (Clotting Cascade)	3. Integrin signaling	3. Extrinsic Prothrombin Activation Pathway
4. Response to elevated platelet cytosolic Ca ²⁺	4. Regulation of TLR by endogenous ligand	4. LXR/RXR Activation
5. Coagulation System	5. Integrin cell surface interactions	5. Coagulation System

Results – Acute Phase Response Signaling

Acute Phase Response Signaling: Rapid inflammatory response

Notable protein: Serum amyloid A (SAA)

- Apolipoprotein; regulator of cell-cell communication, inflammatory, immunologic, neoplastic, protective pathways

Figure 1: Schematic diagram of the Acute Phase Response Signaling pathway. The pathway starts with the activation of the Toll-like receptor (TLR) by endogenous ligands, leading to the activation of the MyD88-dependent signaling pathway. This results in the activation of the transcription factor NF-κB, which then induces the expression of SAA.

Results – Formation of Fibrin Clot (Clotting Cascade)

Formation of Fibrin (Clotting Cascade): conversion of fibrinogen to fibrin for enzymatic cascade of blood coagulation, essential for hemostasis (stopping of bleeding) and thrombosis (vascular obstruction)

Figure 1: Schematic diagram of the Fibrin Clotting Cascade. The cascade starts with the activation of the Tissue Factor (TF) by the Tissue Factor F1 (TFF1), leading to the activation of the Factor VII (F7) to Factor VIIa (F7a). F7a then activates the Factor X (F10) to Factor Xa (F10a), which in turn activates the Factor II (F2) to Factor IIa (F2a). F2a then activates the Factor I (F1) to Factor Ia (F1a), which finally leads to the formation of the Fibrin Clot.

Conclusion

- A leading cause of cancer death, PDAC is
- Pancreatitis not only shares
- In this study



Conclusions & Future Directions

- Prevalence of the EGFR and ALK gene mutations amongst study participants varied by about 5% each from what they were reported to be in literature
- Those with EGFR mutation
 - Higher number of relatives with LC
 - Earlier age of onset
 - Different types of mutations were observed: exon 19 deletion, exon 20 insertion, and p.T790M mutation
- Participants tested positive for the ALK gene despite being one of the most common genes tested for

trans
mutational analysis

31



Giancarlo Lara^{1,§}, Hirotomo Dochi^{2,3,§}, Janardhan Avilala^{2,3,§}, Hong Liu^{2,3}, and Zhen Lin^{2,3}
¹Louisiana State University, ²Tulane University Health Sciences Center and Tulane Cancer Center, ³Louisiana Cancer Research Center
[§]These authors contributed equally.



Materials and Methods

Satellite DNAs are tandem repetitive noncoding DNA sequences and constitute ~6% of the human genomes[1]. They serve as the main structural components for heterochromatin and centromeres and have long been considered as inert DNA with no support for chromatin at the DNA level. However, recent studies indicate that these repeating blocks can be actively transcribed and produce non-polyadenylated satellite RNAs. Intriguingly, several studies have shown that these satellite RNAs are up-regulated by the largest satellite repeat, alpha-satellite, in human cancer[2, 3]. We recently found that these alpha-satellite RNAs induce double-stranded breaks in the genome and that alpha-satellite RNAs in both normal and cancer cells induce DSBs and that DSB-induced genomic instability and thus is involved in cancer. Together, these results suggest that alpha-satellite RNAs in the process of

Generation of α -SatRNAs expression vectors. The cDNA for α -SatRNAs was first generated by *in vitro* synthesis (Genscript). The cDNA was further amplified by PCR and specific restriction sites were added to both ends of the cDNA fragment. Following restriction digestion, the cDNA for α -SatRNAs was cloned into both retroviral and lentiviral vectors. The established α -SatRNAs expression vectors were purified from the transformed bacteria cells. Sanger sequencing analyses were then performed to verify the plasmid sequences.

In vitro Transfection. Human embryonic kidney (HEK) 293 cells were transiently transfected with the plasmids using calcium phosphate transfection method.

Quantitative reverse transcription PCR (RT-qPCR).

Cell proliferation assay. Cell proliferation was examined by the CellTiter assay (Promega).

Western blotting analysis.

RNAScope assay. Probes targeting α -SatRNA transcripts were designed and synthesized by ACDBio. To detect α -SatRNA transcript at the single-cell level, RNAScope assay was conducted.

Figure 2. Project overview.

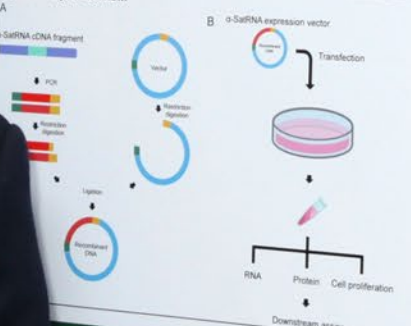


Figure 3. Establishment of α -SatRNA expression systems.

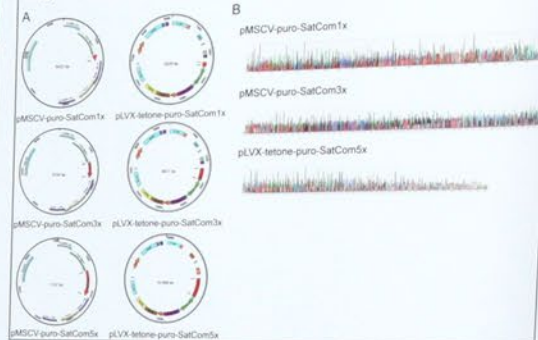


Figure 4. Transient expression of α -SatRNAs in 293 cells.

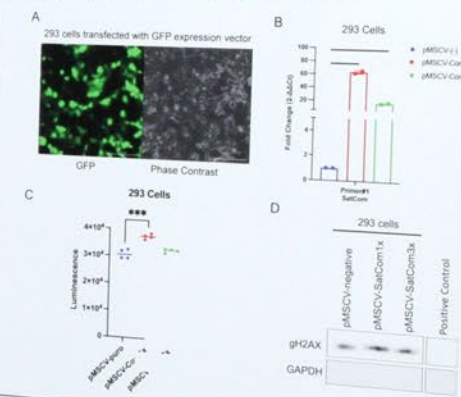


Figure 5. Increased levels of α -SatRNAs in lymphoma cells carrying lytic EBV infection.



Conclusions

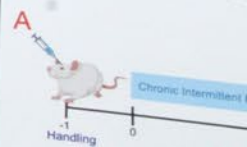
LSU
School of

Introduct

- Humans with alcohol use disorder (AUD) show withdrawal (WD), which is associated with hyperactivity in the VTA.
- The neurobiology underlying WD involves the VTA and the nucleus accumbens (NAc).
- VTA is associated with reward and addiction.
- Cerebellum is associated with emotion and learning.
- Previous work has demonstrated that alcohol WD in a rat model is associated with hyperactivity in the VTA.
- We hypothesized that inhibition of VTA activity would reduce WD-like behavior of dependent rats.
- To test this hypothesis, we used a novel method of projecting VTA neurons and recording their activity.

Methods

- We first analyzed existing data on how these parameters influence behavior
- We used a dual virus approach to label neurons with an inhibitory designer drug (DREADD), and a cre-dependent inhibitor injected into the VTA of adult mice
- To model alcohol dependence (CIE) to ethanol vapor paradigm: 12 hours a day and pure air for 12 hours
- Blood alcohol concentrations: 150-300 mg/dL
- Following 4 weeks of vapor exposure, we observed a change in behavior in an elevated plus maze
- To inhibit the VTA-CeA circuit, we used a designer drug that selectively inhibits GABAergic neurons minutes prior to behavioral tests
- DCZ: designer drug that selectively inhibits GABAergic neurons
- Brains were sectioned to confirm inhibition of cells using phosphorimager





Socio-economic Factors and Racial Disparities That Influence Stage Diagnosis of Cervical Cancer

Aliyah R. Richardson, Lauren S. Maniscalco, MPH,
Almetra A. Granger, MPH, Carleigh W. Baudoin, MPH
Xiao-Cheng, MD, MPH

Louisiana State University Health Sciences Center, School of Public Health,

Louisiana Breast and Cervical Cancer Health Program



LOUISIANA CANCER
RESEARCH CENTER

Introduction

Cervical cancer is an on-going public health concern in Louisiana, as it is ranked 10th in the incidence rate and 5th in the mortality rate in the US. Despite the availability of primary preventative methods, various cervical incidence and mortality rates are still high among Louisiana women.

Cervical Cancer is not only preventable, but early-detection can be achieved by utilizing HPV and Pap Smear tests. However, cervical cancer data between 2016 and 2021 from the Louisiana Tumor Registry, indicates that over 50% of women with cervical cancer were diagnosed at regional and distant stages. The 5-year survival rates associated with late-stage diagnoses are 58% and 16%, respectively, much lower than 88% among those diagnosed at the localized stage.

Moreover, prior research has indicated that socio-demographic barriers impact the cervical cancer stage at diagnosis. While the Louisiana Breast and Cervical Cancer Health Program (LBCCCHP) is set to participate in the nationwide cervical elimination initiative, our research intends to provide valuable data for this effort.

Objectives

- Assess the impact of urban-rural and poverty status of non-Hispanic Black (NHB) and non-Hispanic White (NHW) women.
- Identify underserved areas and populations for the Louisiana's cervical cancer elimination initiative.

Methods

Data Sources:

- Louisiana Tumor Registry collected data in the SEER* Stat Research Plan analytic dataset.
- Louisiana Data Visualization Tool

Eligibility Criteria:

- Louisiana women aged 15 and older diagnosed with invasive cervical cancer between 2016 and 2021.

Variables: Combined...

Results

Metro vs. Non-Metro:

In both Non-Hispanic White (NHW) and Non-Hispanic Black (NHB) populations, metropolitan (metro) regions show a higher percentage of early-stage diagnoses compared to non-Metro regions, (Table 1). NHB women had a much lower percentage of localized diagnosis than their NHW counterparts: 36.1% vs. 47.4% in Metro regions and 31.0% vs. 45.0% in non-metro regions.

Table 1. Cervical Cancer Stage Distribution in Metro and Non-Metro Regions for NHB and NHW Women, Louisiana, 2004-2021

Stage	Non-Hispanic White				Non-Hispanic Black			
	Metro		Non-Metro		Metro		Non-Metro	
	Count	%	Count	%	Count	%	Count	%
Localized	805	47.4	200	45.0	451	36.1	86	31.0
Regional	594	35.0	158	35.6	519	41.6	121	43.7
Distant	214	12.6	63	14.2	197	15.8	55	19.9
Unknown	86	5.1	23	5.2	81	6.5	15	5.4
All	1,699	100.0	444	100.0	1,248	100.0	277	100.0

High poverty vs. Low Poverty:

NHB women had a lower percentage of localized cervical cancer than NHW women regardless of poverty status (35.2% vs. 46.9%) (Table 2). In either high or low-poverty regions, NHB women were less likely than their NHW counterparts to be diagnosed with localized cervical cancer. The percentage of localized cervical cancer among NHB women in low-poverty regions was even lower than that among NHW women in high-poverty regions.

Table 2. Cervical Cancer Stage Distribution in High Poverty and Low Poverty Parishes for NHB and NHW Women, 2004-2021

Stage	Non-Hispanic White				Non-Hispanic Black			
	Low Poverty		High Poverty		Low Poverty		High Poverty	
	Count	%	Count	%	Count	%	Count	%
Localized	667	48.3	338	44.4	200	35.2	86	31.0
Regional	594	35.0	158	35.6	519	41.6	121	43.7
Distant	214	12.6	63	14.2	197	15.8	55	19.9
Unknown	86	5.1	23	5.2	81	6.5	15	5.4
All	1,699	100.0	444	100.0	1,248	100.0	277	100.0

Conclusion

NHB women are more likely to be diagnosed with regional and distant stages of cervical cancer in comparison to NHW regardless of whether they live in metro or non-metro regions.

Women in non-metro areas are less likely to be diagnosed with cervical cancer at the localized stage, especially NHB women. The percentage of localized cervical cancer among NHB women in Metro areas is even lower than NHW women in non-metro areas.

Women in high-poverty regions are less likely to be diagnosed with localized cervical cancer than those who reside in low-poverty regions, regardless of race. However, NHB women in high-poverty regions show a lower percentage of being diagnosed at the localized stage compared to NHW women.

This study highlights the importance of focusing on NHB, non-metro, and high-poverty women to eliminate cervical cancer, increase early detection, and improve survival rates in Louisiana. Additionally, it emphasizes the need to target non-metro and high-poverty regions.

Future Implications

The Louisiana Breast and Cervical Cancer Health Program (LBCCCHP) assists in providing low-cost care to low-income, uninsured, and underinsured women throughout the state. This program includes access to cervical screenings and mammograms. In its efforts to eliminate cervical cancer, Louisiana is in the process of developing a state plan similar to Alabama's State Wipeout initiative. This plan includes increasing school-based HPV vaccinations, promoting routine follow-ups, and enhancing the availability of reproductive physicians in underserved communities.

• Adoles
develop
physical
behavior

• Most
adolesc
and add
for the c

• The bec
is a
implicate
negative
withdraw

• Dynorph
peptide f
(KOR).

• Dyn and
state ass

Hypothes
(AIE) indu
is associ
and KOR
female m

Adolescent
Adolescent
either pyraz
ethanol (AIE)

Crotonylation of c-Myc: A Novel Post-Translational Modification Modulating Its Cancer Promoting Activity

Rashmi Srivastava^{1,2,3,4,5}, Nicholas Wallbillich¹, Shelya X Zeng^{1,2,3}, Hua Lu^{1,2,3}
¹Tulane University School of Medicine, Department of Biochemistry & Molecular Biology; New Orleans, LA; ²Tulane Cancer Center; New Orleans, LA; ³Louisiana Cancer Research Center; New Orleans, LA; ⁴Baylor University, Department of Chemistry & Biochemistry; Waco, TX; ⁵Louisiana State University Health Sciences Center; New Orleans, LA

43

Abstract

We are studying the signaling pathways of cancer biology, focused on the molecular and biochemical mechanisms for cell proliferation and tumorigenesis involving the p53 and c-Myc pathways. We were specifically interested in understanding the role of unique post-translational modifications of proteins such as tumor suppressor TP53 and oncoprotein c-Myc in regulation of the transcription factors' functions and cancer biology. Crotonylation of c-Myc was identified by our lab and the addition of crotonic acid (CA) to cancer cells caused a decrease in c-Myc activity and cellular growth, increased chemosensitivity, and decreased stem-cell formation. The mutant, however, has increased proliferation and colony formation capacity. Lentivirus is also being generated for c-Myc and its mutants to generate stable-cell lines to further investigate phenotypes. We identified a novel post-translational modification on c-Myc and early work shows a modulatory effect on the protein's cancer-promoting activity.

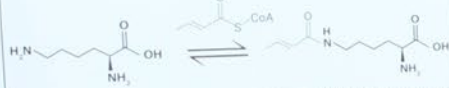


Fig. 1: Reaction scheme of lysine crotonylation. A crotonyl group, conjugated to Coenzyme A (CoA), is enzymatically transferred to lysine residues on both histone and non-histone proteins.

Introduction

Background

Post-Translational Modifications (PTMs) are rapid, reversible changes to the side chain amino acids of proteins. PTMs can affect protein function by activating, degrading, or relocating them, often altering their interactions with other proteins in the process.



Fig. 2: Types of PTMs and the role of Myc in hallmarks of cancer. Short-chain fatty acids (SCFAs) are produced by the gut microbiome and have been shown to have anti-cancer effects due to their ability to suppress tumor growth and cancer cell metastasis. c-Myc is a transcription factor that is estimated to regulate ~10% of the genome and it structurally forms a heterodimer with MAX.

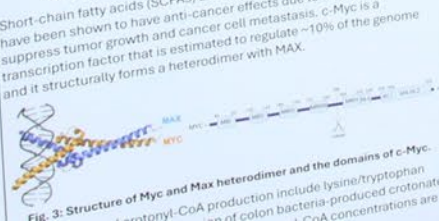


Fig. 3: Structure of Myc and Max heterodimer and the domains of c-Myc. Crotonyl-CoA production include lysine/tryptophan and the addition of crotonic acid (CA) to cancer cells caused a decrease in c-Myc activity and cellular growth, increased chemosensitivity, and decreased stem-cell formation.

Methodology

Immunoprecipitation & Cycloheximide Chase (CHX)

To purify antigens using specific antibodies, immunoprecipitation (IP) is used. To measure steady state protein stability and half life of c-Myc, time-points were taken every hour for 3 hours after the drug CHX was added to the plates for the CHX chase.



The samples prepared from IP & the CHX chase were run on western blots to analyze protein expression and identify specific proteins. The proteins were extracted and separated by gel electrophoresis, transferred to a membrane, blocked to prevent non-specific binding, probed with a primary antibody, then a secondary antibody with a detectable marker, and finally visualized to detect the target protein.



Mass Spectrometry & PCR Mutagenesis

After overexpressing c-Myc and adding CA, the cells are harvested for immunoprecipitation. The samples are then run on an SDS-page gel in order to separate the proteins based on their molecular weight. The correct sized band is cut and digested to then run on the liquid chromatography-mass spectrometry (LC-MS).

After the correct crotonylation sites were identified, PCR mutagenesis was used to create mutants at eight different sites.

After the correct crotonylation sites were identified, PCR mutagenesis was used to create mutants at eight different sites.

Cell Viability & Proliferation

To measure cell proliferation and cell viability, the H1299 cells were plated in a 96 well plate. The H1299 cells were placed in the incubator to measure the confluence every 2 hours for 72 hours. The time was normalized with the 0-time point.

Determining Crotonylation of c-Myc

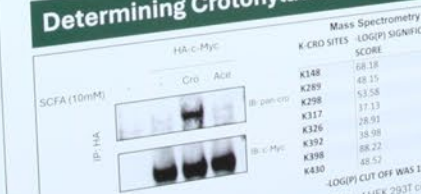


Fig. 4: Identification of c-Myc crotonylation: Western blots of HEK 293T cells with a pan-crotonylation antibody (purified from crotonylated histones) showed that c-Myc is crotonylated and is distinct from these results. A total of 8 crotonylation sites were identified on c-Myc that span the mid portion to the C-terminus of the protein. Point mutations were then constructed using PCR mutagenesis to generate K to R mutants. The 2R and 8R mutant sites were identified to ablate western signal.

Results

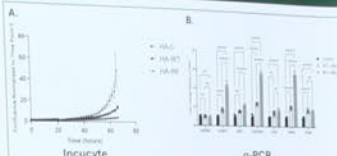


Fig. 5: Mutant c-Myc is more active than wild type c-Myc: A: H1299 cells were transiently transfected with 1 µg of plasmid and confluence was measured every 2 hours for ~72 hours on the incubator. Mutant HA-8R-c-Myc was shown to proliferate faster than the WT. B: Quantitative chain polymerase reaction (q-PCR) used to measure cell cycle gene expression of downstream cell-cycle related c-Myc targets also showed increased activation by the mutant compared to the control and WT.

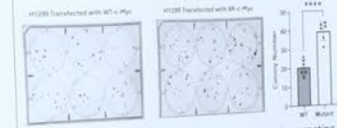


Fig. 6: Mutant c-Myc is more active than wild type c-Myc in promoting colony formation: H1299 cells were transfected with WT-c-Myc and mutant 8R-c-Myc. About 5000 cells were plated in 6-well dishes to measure if the cells were able to survive and grow colonies. The medium was changed every 3 to 4 days for 10 days and the plates were then stained with crystal violet. Quantification of colonies is shown in the graph on the right (**** indicates that P-value is 0.0001).



Fig. 7: Mutant c-Myc is ubiquitinated more, so it is less stable than wild type c-Myc: A: H1299 cells were transfected with 1 µg His-tagged HA-WT-c-Myc or HA-8R-c-Myc. The lysates were immunoprecipitated with anti-His antibody and analyzed on a Western blot. B: Pulse chase assay. Time points were taken every 10 minutes after the addition of the CHX drug was added to the cells. Protein levels were detected by WB with indicated antibodies.

Conclusion & Future Directions

Crotonylation, a novel post-translational modification, on the oncoprotein c-Myc. Phenotype studies indicate this PTM effect on the oncogenic functions of c-Myc. Mechanistic studies indicate the mutant displays replicating phenotype during cell cycle. Future directions include replicating phenotype during cell cycle as well as further mechanistic work to understand the relationship between the wild type and crotonylation modified proteins.

Predictors of Reunification for Children and Their Parents in Cases Involving Parental Substance Use in Louisiana

Jaclyn Rosalie Hodges, Amy Dickson Psy D, Amy Rinner-Clomburg, Psy D, Sebastian Del Corral Winder, Psy D
Louisiana State University Health Sciences Center, Department of Psychiatry



24

Introduction

Substance use inhibits a parent's ability to care for their children, putting them at risk for neglect, maltreatment, danger, and possibly foster care. It is estimated that 50-80% of children in foster care have at least one parent with a history of Substance Use Disorder (SUD) [1]. The Department of Child and Family Services (OCFS) works with families whose children are in foster care to support the goal of reunification. Parents attempt to reunite with their children to protect their children. The LSUHSC Infant Team evaluates parent-child relationships and provides support services to these families. Research shows that parents who receive treatment and support services are more likely to reunite with their children. The goal of this study was to identify predictors of reunification for children and their parents in cases involving parental substance use in Louisiana.

Data



Figure 1: Mothers with and without SUDs and Reunification

Results

Results (n = 178): 37.1% (66) of mothers with SUDs achieved reunification compared to 50.0% (50) of mothers without SUDs. For mothers with SUDs who were reunified, the median time to reunification was 12.5 months (IQR = 6.0-24.0). For mothers without SUDs who were reunified, the median time to reunification was 8.0 months (IQR = 4.0-16.0). The difference in time to reunification was statistically significant (p = 0.001). The difference in the percentage of mothers who achieved reunification was also statistically significant (p = 0.001).

Figure 2: Fathers with and without SUDs and Reunification



Figure 3: Mothers with and without SUDs and Reunification



Figure 4: Fathers with and without SUDs and Reunification

Figure 5: Mothers with and without SUDs and Reunification

Figure 6: Fathers with and without SUDs and Reunification

Figure 7: Mothers with and without SUDs and Reunification

Figure 8: Fathers with and without SUDs and Reunification

Figure 9: Mothers with and without SUDs and Reunification

Figure 10: Fathers with and without SUDs and Reunification

Figure 11: Mothers with and without SUDs and Reunification

Figure 12: Fathers with and without SUDs and Reunification

Overcoming Multidrug Resistance in Breast Cancer: Targeting MRP Proteins for Enhanced Therapeutic Efficacy

Camryn Tims, Rajib Biswas, Treiveanna Jenkins, Anup Kundu PhD.
Biology Department, Xavier University; Tulane University Health Sciences Center



Introduction

In this project, the MDR proteins will be targeted as the major resistant protein in the cancer cell lines. When MRP-1/P-gp is highly expressed, it creates an extremely resistant cell environment for the breast cancer cells. This protein has the ability to dispel a huge list of anti-cancer drugs including doxorubicin. We anticipate that knocking down MRP-1/P-gp by siRNA encapsulated nanoparticles could enhance the delivery of doxorubicin (Dox) into the breast cancer cells. The preliminary study has been focused on the development of an aptamer-labeled nanoparticle system for effective delivery of MRP-1/P-gp siRNA into breast cancer cells.

Exp. Design

For targeted delivery, Aptamer-A6 has been used which can bind to Her-2 receptors on breast cancer cells. The particles were prepared by high pressure homogenization (HPH) using different amount of DOTAP, cholesterol, PLGA or PLGA-PEG and Mal-PEG. After siRNA encapsulation, the particles were incubated with aptamer-A6 for surface labeling. The liposomal particles were characterized for their size, surface charge and cytotoxicity. The delivery of siRNA into different breast cancer cells has been assessed by immunofluorescence and FACS analysis.



Figure 1. Schematic diagram showing the organization of the nanoparticles

Data

Figure 2. The expression of MRP-1 in 4T1-R and 4T1-S breast cancer cells by immunofluorescence.

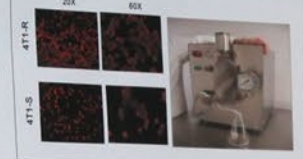


Figure 3. Comparison of particle size (a) and zeta potential (b) between blank and siRNA nanoparticles (with aptamer)

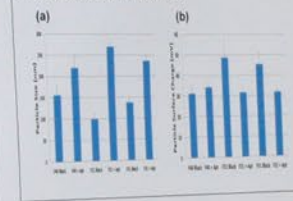


Figure 4. The expression of Her-2 and P-gp (left panel) and the knockdown of P-gp in 4T1-R, SKBR-3 and MCF-7 cells with/without aptamer labeled nanoparticles (right panel).



Assays

Western Blot

Western Blot tests were conducted to confirm the presence and size of the MRP-1 (Multi-Drug Resistant Protein) in the dox-resistant cells.

qPCR

Additionally, qPCR tests were run to identify and compare RNA concentrations amongst the 4T1-R and MDA-231 cell lines.

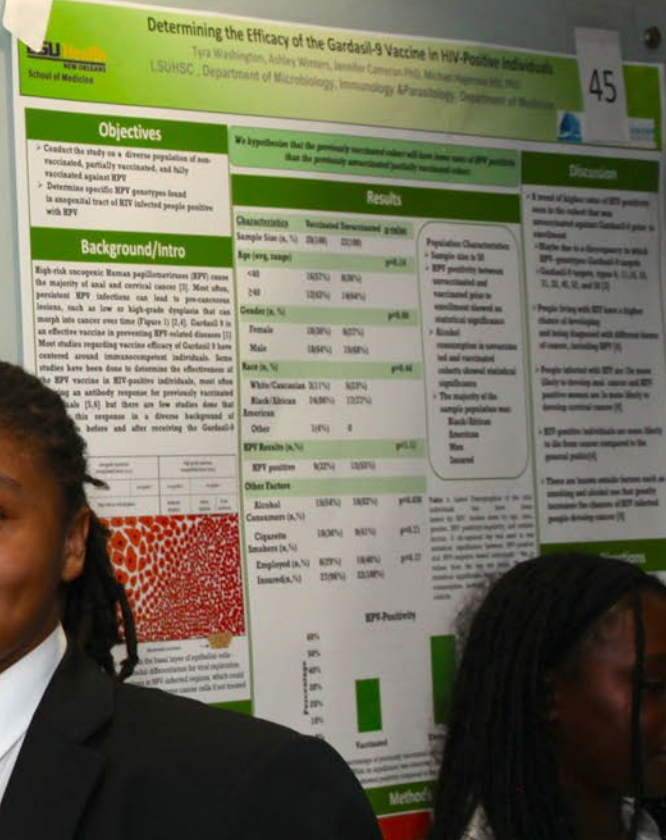
Conclusion

The prior study has shown that the uptake of Dox by Dox-resistant 4T1-R is significantly less than Dox-sensitive 4T1-S which is partly attributed to the higher expression of drug-efflux pump (i.e., ABC transporter proteins P-gp, MRP-1, BCRP, etc.) on the surface of the resistant cells. The targeted knockdown of P-gp or MRP-1 has been enhanced when the particles carrying P-gp siRNA or MRP-1 siRNA, respectively were labeled with aptamer. Concurrently, the uptake of Dox into the Dox-resistant 4T1-R breast cancer cells has increased significantly when the MDR proteins were knocked down by appropriate siRNA-encapsulated aptamer-labeled nanoparticles.

References

1. Patel, D., Chandra, S., Garg, A., Kundu, A. (2017) Aptamer-Targeted Nanoparticles for Overcoming Multidrug Resistance in Breast Cancer: Targeting MRP Proteins for Enhanced Therapeutic Efficacy.
2. Kundu, A., et al. (2018) Targeted delivery of siRNA against MRP-1 in breast cancer cells using aptamer-labeled nanoparticles.
3. Chandra, S., Kundu, A., Garg, A., Patel, D. (2019) Targeted delivery of siRNA against MRP-1 in breast cancer cells using aptamer-labeled nanoparticles.

This research project was supported by the Stanley S. Scott Cancer Center.



Conduct the study on a diverse population of non-vaccinated, partially vaccinated, and fully vaccinated against HPV
 Determine specific HPV genotypes found in anogenital tract of HIV infected people positive with HPV

Background/Intro

High-risk oncogenic Human papillomaviruses (HPV) cause the majority of anal and cervical cancer [3]. Most often, persistent HPV infections can lead to pre-cancerous lesions, such as low or high-grade dysplasia that can morph into cancer over time (Figure 1) [2,4]. Gardasil 9 is an effective vaccine in preventing HPV-related diseases [1]. Most studies regarding vaccine efficacy of Gardasil 9 have centered around immunocompetent individuals. Some studies have been done to determine the effectiveness of the HPV vaccine in HIV-positive individuals, most often showing an antibody response for previously vaccinated individuals [5,6] but there are few studies done that observe this response in a diverse background of individuals before and after receiving the Gardasil-9 vaccine.

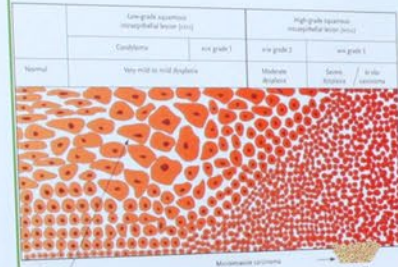


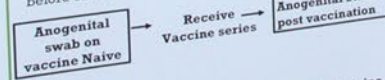
Figure 1. HPV infection occurs in the basal layer of epithelial cells - oftentimes dysregulating epithelial differentiation for viral replication. This leads to low-grade dysplasia in HPV-infected regions, which could advance to high-grade dysplasia and become cancer cells if not treated early.

Enrollment Criteria

Approximately 150 HIV-positive adults, under informed consent, were enrolled in the study at the University Medical Center (UMC) with the following:

- A blood CD4+ T cell count of ≥ 200 cells/mL
- HIV viral load <1000 genome copies/mL
- If taking antiretroviral medicine then stable on it for ≥ 3 months

1st Cohort
 Not previously and/or partially vaccinated with Gardasil before enrollment



2nd Cohort
 Previously received all 3 doses of the Gardasil vaccine

Low recruitment of HPV vaccine naive individuals led to another sector of enrolled individuals. People with all three doses of the HPV vaccine get swabs of DNA taken from the anogenital region for HPV genotyping and testing of their antibodies. Follow-ups occur every 6 months for more swab extracts.

We hypothesize that the previously vaccinated cohort will have lower rates of HPV positivity than the previously unvaccinated/partially vaccinated cohort.

Results

Characteristics	Vaccinated	Unvaccinated	p-value
Sample Size (n, %)	28(100)	22(100)	
Age (avg, range)			
<40	16(57%)	8(36%)	p=0.14
≥ 40	12(43%)	14(64%)	
Gender (n, %)			
Female	10(36%)	6(27%)	p=0.60
Male	18(64%)	15(68%)	
Race (n, %)			
White/Caucasian	3(11%)	5(23%)	p=0.44
Black/African American	24(86%)	17(77%)	
Other	1(4%)	0	
HPV Results (n, %)			
HPV positive	9(32%)	12(55%)	p=1.11
Other Factors			
Alcohol Consumers (n, %)	15(54%)	18(82%)	p=0.036
Cigarette Smokers (n, %)	10(36%)	9(41%)	p=0.71
Employed (n, %)	8(29%)	10(46%)	p=0.17
Insured (n, %)	27(96%)	22(100%)	

Population Characteristics
 Sample size is 50
 HPV positivity between unvaccinated and vaccinated prior to enrollment showed no statistical significance
 Alcohol consumption in unvaccinated and vaccinated cohorts showed statistical significance
 The majority of the sample population was: Black/African American Men Insured

Table 1. Listed Demographics of the total individuals that have been tested for HPV, broken down by age, race, gender, HPV positivity/negativity, and outside factors. A chi-squared test was used to test statistical significance between HPV-positive and HPV-negative tested individuals - the p-values from the test are listed. The only statistical significance found was from alcohol consumption between the two prospective cohorts.

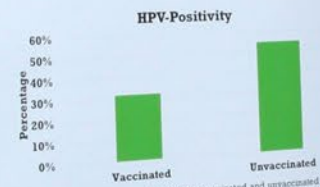


Figure 2. A bar chart of the percentage of previously vaccinated and unvaccinated people before enrollment that expressed HPV-positivity. While no significance was observed, there is a difference within the cohorts, as more than half of the unvaccinated showed positivity compared to the vaccinated.

Methods

PCR		Gel Electrophoresis	
Primer Sets	Size Fragment		
HPV L1 gene	448bp	MY11-5' - GCM CAG GGG CAT AAT GG - 3'	MY9-5' - CGT CCM ARR GGA WAC TGA TC - 3'
		PC04-5' - GAA GAG CCA AAG ACA GGT AC - 3'	PC04-3' - GAA GAG CCA AAG ACA GGT AC - 3'
β -globin	268bp	GH20-5' - CAA CTT CAT CCA GGT TCA CC - 3'	

Table 2. A dual primer PCR was completed on the extracted swab DNA from the anal and vaginal region. MY9/MY11, a degenerate primer set, was utilized to detect various HPV genotypes from the sampled Genomes. DNA. A β -globin primer set, PC04/GH20, was used to make sure human DNA was present.

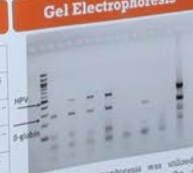


Figure 3. Gel Electrophoresis was utilized to separate the DNA fragments from the dual primer PCR. Negative and positive controls were also run under the same analysis with the cohort samples to ensure quality of the results.

Discussion

- A trend of higher rates of HIV-positivity seen in the cohort that was unvaccinated against Gardasil-9 prior to enrollment
- Maybe due to a discrepancy in which HPV genotypes Gardasil-9 targets
- Gardasil-9 targets, types 6, 11, 16, 18, 31, 33, 45, 52, and 58 [3]
- People living with HIV have a higher chance of developing and being diagnosed with different forms of cancer, including HPV [4]
- People infected with HIV are 15x more likely to develop anal cancer and HIV-positive women are 7x more likely to develop cervical cancer [4]
- HIV-positive individuals are more likely to die from cancer compared to the general public [4]
- There are known outside factors such as smoking and alcohol use that greatly increases the chances of HIV infected people develop cancer [4]

Future Directions

- This study will continue to progress with the extraction and testing of the rest of the swab samples
- HPV positive samples will be sent for genotyping through My-Seq Platform
- A comparison will likely be done with non-immune deficient population data to note any discrepancies

References

1. Centers for Disease Control and Prevention. HPV Vaccination: What You Need to Know. 2018. Available from: <https://www.cdc.gov/hpv/hpvvaccine/index.html>
2. American Cancer Society. HPV and Cervical Cancer. 2018. Available from: <https://www.cancer.org/cancer/hpv/cervical-cancer/about-hpv/cervical-cancer-facts.html>
3. American Cancer Society. HIV and Cancer. 2018. Available from: <https://www.cancer.org/cancer/hiv-and-cancer/about-hiv/hiv-and-cancer-facts.html>
4. American Cancer Society. HIV and Cancer. 2018. Available from: <https://www.cancer.org/cancer/hiv-and-cancer/about-hiv/hiv-and-cancer-facts.html>

Acknowledgements

I want to acknowledge LCHC for funding this research. I also want to thank the Stanley S. Scott Cancer Center for creating and aiding in this project supported by funding from Merck (MSRP1476).

This research project was supported by the Stanley S. Scott Cancer Center.